

High stability and low noise laser-diode end-pumped Nd: YAG ceramic passively *Q*-switched laser at 1123 nm based ona $Ti_3C_2T_x$-PVA saturable absorber

Jia-Le Yan(闫佳乐), Ben Li(李奔), Guo-Zhen Wang(王国珍), Shun-Yu Yang(杨顺宇),Bao-Le Lu(陆宝乐), and Yang Bai(白杨)

Citation: Chin. Phys. B, 2023, 32 (**11**): 114212. DOI: 10.1088/1674-1056/acf495
Journal homepage: http://cpb.iphy.ac.cn; http://iopscience.iop.org/cpb

What follows is a list of articles you may be interested in

Pulse generation of erbium-doped fiber laser based on liquid-exfoliated $FePS_3$

Qing Yin(阴晴), Jin Wang(汪进), Xin-Yao Shi(史鑫尧), Tao Wang(王涛), Jie Yang(杨洁), Xin-Xin Zhao(赵新新), Zhen-Jiang Shen(沈振江), Jian Wu(吴坚), Kai Zhang(张凯), Pu Zhou(周朴), Zong-Fu Jiang(姜宗福)
Chin. Phys. B, 2019, 28 (**8**): 084208. DOI: 10.1088/1674-1056/28/8/084208

Er^{3+},Yb^{3+}:glass-Co^{2+}:$MgAl_2O_4$ diffusion bonded passively Q-switched laser

Yan Zou(邹岩), Yong-Ling Hui(惠勇凌), Jin-Lu Cai(蔡瑾鹭), Na Guo(郭娜), Meng-Hua Jiang(姜梦华), Hong Lei(雷訇), Qiang Li(李强)
Chin. Phys. B, 2017, 26 (**9**): 094206. DOI: 10.1088/1674-1056/26/9/094206

1.5-MHz repetition rate passively Q-switched Nd: YVO_4 laser based on WS_2 saturable absorber

Xi Wang(王茜), Lu Li(李璐), Jin-Ping Li(李金萍), Yong-Gang Wang(王勇刚)
Chin. Phys. B, 2017, 26 (**4**): 044203. DOI: 10.1088/1674-1056/26/4/044203

Tunable Nd, La: SrF_2 laser and passively Q-switched operation based on gold nanobipyramids saturable absorber

Feng Zhang(张峰), Hua-Nian Zhang(张华年), Dan-Hua Liu(刘丹华), Jie Liu(刘杰), Feng-Kai Ma(马凤凯), Da-Peng Jiang(姜大朋), Si-Yuan Pang(逄思远), Liang-Bi Su(苏良碧), Jun Xu(徐军)
Chin. Phys. B, 2017, 26 (**2**): 024205. DOI: 10.1088/1674-1056/26/2/024205

1.12-W Q-switched Yb:KGW laser based on transmission-type Bi_2Se_3 saturable absorber

Liu Jing-Hui (刘京徽), Tian Jin-Rong (田金荣), Hu Meng-Ting (胡梦婷), Xu Run-Qin (徐润亲), Dou Zhi-Yuan (窦志远), Yu Zhen-Hua (于振华), Song Yan-Rong (宋晏蓉)
Chin. Phys. B, 2015, 24 (**2**): 024215. DOI: 10.1088/1674-1056/24/2/024215

SPECIAL TOPIC — Celebrating the 100th Anniversary of Physics Discipline of Northwest University

High stability and low noise laser-diode end-pumped Nd: YAG ceramic passively Q-switched laser at 1123 nm based on a $Ti_3C_2T_x$-PVA saturable absorber

Jia-Le Yan(闫佳乐)[1], Ben Li(李奔)[1], Guo-Zhen Wang(王国珍)[1], Shun-Yu Yang(杨顺宇)[1], Bao-Le Lu(陆宝乐)[1,2], and Yang Bai(白杨)[1,2,†]

[1] *Institute of Photonics & Photon-Technology, Northwest University, Xi'an* 710127, *China*
[2] *Shaanxi Engineering Technology Research Center for Solid State Lasers and Application, Xi'an* 710127, *China*

(Received 3 July 2023; revised manuscript received 28 August 2023; accepted manuscript online 29 August 2023)

We report a high repetition frequency, high power stability and low laser noise laser-diode (LD) end-pumped Nd: YAG ceramic passively Q-switched laser at 1123 nm based on a $Ti_3C_2T_x$-polyvinyl alcohol (PVA) film as a saturable absorber (SA). A Brewster polarizer (BP) and a birefringent crystal (BC) are incorporated to enable frequency selection and filtering for the passively Q-switched 1123 nm pulsed laser to improve the power stability and reduce the noise. When the pump power is 5.1 W, an average output power of 457.9 mW is obtained, corresponding to a repetition frequency of 1.09 MHz, a pulse width of 56 ns, a spectral line width of 0.65 nm, a power instability of ±0.92%, and a laser noise of 0.89%. The successful implementation of the "$Ti_3C_2T_x$-PVA film passively Q-switching" combined with "frequency selection and filtering of BP + BC" technology path provides a valuable reference for developing pulsed laser with high repetition frequency, high stability and low noise.

Keywords: passively Q-switched, pulsed laser at 1123 nm, $Ti_3C_2T_x$-PVA film, frequency selection and filtering of Brewster polarizer (BP) and birefringent crystal (BC)

PACS: 42.55.Xi, 42.60.Gd, 42.60.Lh **DOI:** 10.1088/1674-1056/acf495

1. Introduction

The 1123 nm near-infrared laser, as widely recognized, generated through stimulated radiation from the $^4F_{3/2}$ energy level to the $^4I_{11/2}$ energy level in Nd: YAG crystal or Nd: YAG ceramic, has been extensively applied in specialized fields such as biotechnology, laser displays, and frequency conversion.[1–3] For example, 1123 nm laser has been used to remote sensing atmospheric water vapor concentration. In the domains of RGB color displays, printing, and data recording, the 1123 nm laser serves as a pump source for thulium up-conversion fiber lasers to generate blue-light emission at 481 nm.[4–6] Additionally, the 561 nm yellow-green laser generated by the frequency doubling 1123 nm is an ideal laser source for dermatology, bioluminescence detection, and holographic storage.[7–9]

However, the absence of active frequency selection and filtering results in significant output noise in the 1123 nm pulsed laser. This is due to the fact that the Nd: YAG crystal or Nd: YAG ceramic generates three spectral lights at 1112 nm, 1116 nm and 1123 nm through stimulated emission.[10–12] The stimulated-emission cross section values are similar for 1123 nm and the other two spectral lights, and they have a small wavelength difference. Achieving simultaneous suppression of the spectral lights at 1112 nm and 1116 nm using anti-reflection coatings is not feasible.

To address mode competition from 1112 nm and 1116 nm, the implementation of Fabry–Perot (F–P) etalons or birefringent crystal (BC) placed according to Brewster angle proves effective in suppression.[13–15] However, the higher losses associated with the use of F–P etalons often result in lower output power and optical-to-optical conversion efficiency of the 1123 nm laser. When using BC, it becomes critical to accurately adjust the Brewster angle and the angle between the BC surface and the optical axis of the 1123 nm spectral light. The intricacies involved in these adjustments often present challenges in achieving a stable output for the 1123 nm laser.

As an emerging two-dimensional material in recent years, titanium carbide $Ti_3C_2T_x$ film has garnered significant attention in the field of passively Q-switched laser due to its advantages such as controllable electronic band structure, a wide range of nonlinear optical response, high optical damage threshold, and large nonlinear absorption coefficient. However, the majority of existing reports on $Ti_3C_2T_x$ two-dimensional film used as a SA in passively Q-switched lasers focus on wavelengths at 1.06 μm, 1.3 μm, 2.73 μm, and 3 μm.[16–19] Few of the reports are about $Ti_3C_2T_x$ used as an SA for passively Q-switched lasers at 1123 nm.

Here, we report a first demonstration, to the best of our knowledge, of a passively Q-switched pulsed laser at 1123 nm using a "$Ti_3C_2T_x$-PVA film passively Q-switching" combined

†Corresponding author. E-mail: by@nwu.edu.cn

© 2023 Chinese Physical Society and IOP Publishing Ltd

with "frequency selection and filtering of Brewster polarizer (BP) + BC" technology path. A new two-dimensional (2D) material $Ti_3C_2T_x$-PVA film was employed to demonstrate the passively *Q*-switched pulsed laser at 1123 nm with high repetition frequency. The combined use of BP and BC reduced the number of longitudinal modes of the passively *Q*-switched pulsed laser at 1123 nm in the cavity while suppressing intracavity oscillations in two spectral lines at 1112 nm and 1116 nm, which was conducive to the improvement of the power stability and the reduction of its noise. A passively *Q*-switched pulsed laser at 1123 nm with an average power of 457.9 mW, a pulse width of 56 ns, a power-instability of ±0.92%, and a laser noise of 0.89% width at the repetition frequency of 1.09 MHz were obtained.

2. Material fabrication and characterization

The process of preparing $Ti_3C_2T_x$-PVA film is as follows: Initially, 1.0 g of LiF powders were placed in 20 mL of HCl solution (10 mol/L) and stirred continuously. Once the LiF powders were completely dissolved, 1.0 g of Ti_3AlC_2 powders were slowly introduced to the above solution and the reaction was carried out at 36 °C for 36 h. Next, the solution was further diluted with deionized water and subjected to multiple centrifugation cycles at a centrifuge speed of 5000 r/min for 5 min each until the pH of the supernatant reached approximately 6–7. The resulting precipitate was then transferred to a vacuum drying oven, where it was dried at 40 °C for 24 h, yielding the $Ti_3C_2T_x$ powders.

Secondly, 50 mg of $Ti_3C_2T_x$ powders were introduced in a mixed solution comprising 150 mL of deionized water and 150 mL of anhydrous ethanol. The mixed solution was subjected to 30 min of continuous sonication to further reduce the number of layers of the $Ti_3C_2T_x$ powders. Subsequently, the sonicated mixed solution was centrifuged for 10 min using a centrifuge at 7000 r/min and then its supernatant containing the $Ti_3C_2T_x$ nanosheets was extracted.

The supernatant was analyzed using confocal Raman spectroscopy excited with a 1064 nm laser. Figure 1(a) illustrates the presence of four characteristic peaks at 148 cm^{-1}, 202 cm^{-1}, 403 cm^{-1}, and 620 cm^{-1}, providing confirmation of the fabricated material being $Ti_3C_2T_x$.[20] The $Ti_3C_2T_x$ nanosheets were characterized using an atomical force microscopy (AFM). As shown in Fig. 1(b), the thickness analyzed from the profile is about 3.5 nm. Based on the research conclusion that the layer spacing of the $Ti_3C_2T_x$ nanosheets is about 0.99 nm,[21] it is concluded that the number of layers of the $Ti_3C_2T_x$ nanosheets prepared in this study is 3–4 layers.

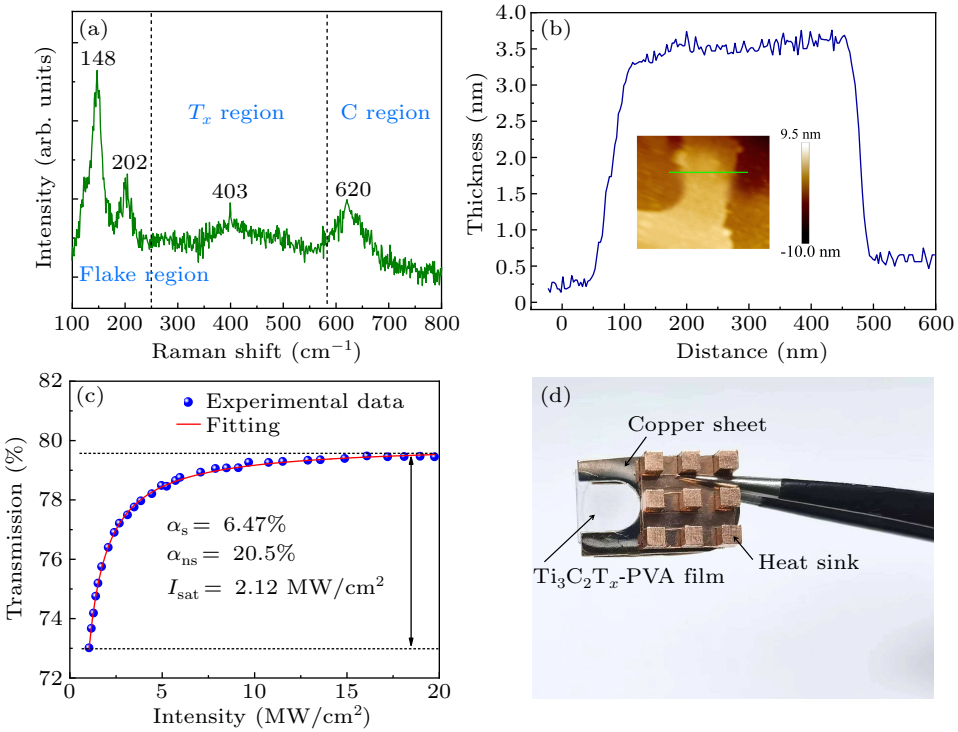


Fig. 1. (a) Raman spectrum for $Ti_3C_2T_x$ nanosheets. (b) Atomic force microscopy (AFM) measured thickness profile of the $Ti_3C_2T_x$ nanosheets along the green line in the inset. (c) Normalized nonlinear optical transmittance measured for $Ti_3C_2T_x$-PVA film based on a balanced twin-detector system by using a 1064 nm laser with 14 ps. (d) Photo of $Ti_3C_2T_x$-PVA film coated sapphire glass with the copper heat sink.

Finally, 0.5 g of PVA powders were dissolved in 50 mL of deionized water at a temperature of 90 °C, and the solution was magnetically stirred for 1 h to fully dissolve the PVA powder. The PVA solution was mixed with the supernatant containing $Ti_3C_2T_x$ at a volume ratio of 1:1 and subjected to continuous sonication for 1 h. The sonicated $Ti_3C_2T_x$-PVA mixed solution was then uniformly spin-coated using a spin coater onto a surface of sapphire glass with a thickness of 0.2 mm. The

coated samples were dried in a thermostatic chamber at 80 °C for 24 h, resulting in the fabrication of a $Ti_3C_2T_x$-PVA film. The thickness of the $Ti_3C_2T_x$-PVA film on the sapphire glass was measured to be 15.3 μm using a thickness gauge.

The transmittance versus illumination intensity of the $Ti_3C_2T_x$-PVA film was obtained using a balanced twin-detector system. The light source of the detection system is a 1064 nm mode-locked fiber laser with a pulse width of 14 ps and a repetition frequency of 28.8 MHz, operating close to 1123 nm. As shown in Fig. 1(c), the transmittance exhibits a trend of first enhancement and then saturation with the pulse intensity, confirming that the $Ti_3C_2T_x$-PVA film can be used as an SA. The nonlinear optical transmittance of the $Ti_3C_2T_x$-PVA film can be fitted using the most common SA model[22]

$$T = 1 - \frac{\alpha_s}{1 + I/I_{sat}} - \alpha_{ns}, \tag{1}$$

where T denotes the transmittance; α_s and α_{ns} denote saturable absorption component (also termed the modulation depth) and non-saturable absorption component, respectively. I and I_{sat} denote the incident light intensity and the saturation light intensity, respectively.

As evident from the results presented in Fig. 1(c), there is a high degree of agreement between the experimental data and Eq. (1). The calculated saturation light intensity and modulation depth of the $Ti_3C_2T_x$-PVA film near 1 μm wavelength are 2.12 MW/cm^2 and 6.47%, respectively. In addition, a thermally conductive copper sheet is attached to each side of the $Ti_3C_2T_x$-PVA film coated sapphire glass, and a square copper heat sink is attached to one of the thermally conductive copper sheets, as shown in Fig. 1(d). This arrangement enhances the natural heat dissipation efficiency and alleviates stability and reliability concerns of the $Ti_3C_2T_x$-PVA film during long-term operation caused by insufficient heat dissipation.

3. Experimental setup

A linear-cavity for a passively Q-switched pulsed laser at 1123 nm using a $Ti_3C_2T_x$-PVA film as an SA is shown in Fig. 2. A Nd: YAG ceramic (2 mm × 2 mm × 6 mm, 0.5 at.% Nd^{3+} doped) was water-cooled at 16 °C and was end-pumped by an 808 nm continuous wave laser-diode (LD) with a total pump power of 5.1 W. Two symmetrically positioned G2 plano-convex lenses were used to collimate and focus the LD pump laser. A focused beam with a focal length of 3.4 mm and a focal spot radius of 250 μm was formed behind the pump surface of the Nd: YAG ceramic. The pumped end surface of the Nd: YAG ceramic was coated with anti-reflection (AR) coatings covering the wavelengths of 808 nm (reflectivity, $R < 1\%$), 946 nm ($R < 5\%$), 1064 nm ($R < 0.5\%$) and 1319 nm ($R < 5\%$), as well as high reflection (HR) coatings covering the wavelength range from 1100 nm to 1130 nm ($R > 99.5\%$). The other end surface was anti-reflection (AR) coated for wavelengths from 1064 nm to 1319 nm ($R < 0.5\%$). Mirror M was the output mirror of the 1123 nm laser. Its intracavity concave surface was coated with AR-coatings covering the wavelength range from 1110 nm to 1125 nm (transmittance, $T \approx 4\%$) and AR-coatings covering the wavelengths of 1064 nm ($R < 5.0\%$), 946 nm ($R < 5.3\%$), and 1319 nm ($R < 7.5\%$). Its plane surface was coated with anti-reflection (AR) coatings the wavelength range from 1064 nm to 1319 nm ($R < 0.6\%$). BP was made of fused quartz glass with a size of 6.0 mm × 6.0 mm × 0.5 mm, while BC is made of quartz crystal with a size of 6.0 mm × 6.0 mm × 2.5 mm. The optical axis of BC was parallel to the diagonal at 45° above its incident surfaces. The transparent surfaces of BP and BC were not coated. The size of the sapphire glass coated with the $Ti_3C_2T_x$-PVA film on one side was 8.0 mm × 8.0 mm × 0.2 mm.

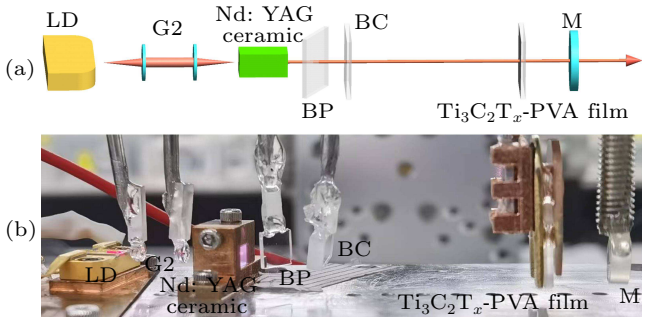


Fig. 2. Experimental setup for (a) structure schematic. (b) Cavity photo.

The thermal focal length of the Nd: YAG ceramic was measured using a dynamic testing method.[23] The results indicated a decrease in the thermal focal length from 900 mm to 500 mm when the pump power of the LD increased from 1 W to 6 W. The cavity structure of the 1123 nm laser was optimized based on the ABCD matrix theory, taking into account the measured thermal lens focal length. Ultimately, the curvature radius of the output mirror M was determined to be 250 mm, and the length of the cavity was 45.2 mm. In the cavity range from the output end surface of the Nd: YAG ceramic to the concave surface of the output mirror M, the distance between the two adjacent optical elements was 4.5 mm, 4.5 mm, 21.0 mm, and 6.5 mm, respectively. When the thermal focal length changed from 900 mm to 500 mm, the stability parameters $(A+D)/2$ of the sagittal and tangential components at 1123 nm within the cavity experienced changes from 0.49 to 0.41 and 0.52 to 0.45, respectively. According to the stable oscillation condition of $|(A+D)/2| < 1$, the cavity is not sensitive to heat.[24]

4. Result and discussion

According to Fresnel's law, non-polarized light at 1123 nm that passes through BP separates into p- and s-polarized light. The reflectivity of the two polarizations on

the BP face can be expressed as follows:[25,26]

$$R_{\rm p} = \frac{{\rm tg}^2(\theta-\omega)}{{\rm tg}^2(\theta+\omega)}, \tag{2}$$

$$R_{\rm s} = \frac{\sin^2(\theta-\omega)}{\sin^2(\theta+\omega)}, \tag{3}$$

where $R_{\rm p}$ and $R_{\rm s}$ denote the reflectivity of p- and s-polarized lights, respectively. θ and ω denote the incident angle and refraction angle of the non-polarized light, respectively.

For BP made of optical quartz glass, the refractive indices (n_i) at 1112 nm, 1116 nm, and 1123 nm are provided by the manufacturer as 1.444, 1.435, and 1.424, respectively. Assuming the refractive index of air as approximately 1, the relationship between Brewster's angle Φ_i, n_i, θ, and ω are as follows based on Brewster's law and the law of refraction:

$$\Phi_i = {\rm arctg}\,(n_i), \tag{4}$$

$$\frac{\sin(\theta)}{\sin(\omega)} = n_i, \tag{5}$$

where i denote the wavelengths of 1112 nm, 1116 nm, and 1123 nm, respectively. The Φ_i can be calculated as 55.31° at 1112 nm, 55.12° at 1116 nm, and 54.92° at 1123 nm using Eqs. (4) and (5), respectively.

As shown in Fig. 3, only the $R_{\rm p}$ of the p-polarized light at 1123 nm is zero at $\alpha = \Phi_{1123} = 54.92°$. The result is that the p-polarized light at 1123 nm only achieves oscillation in the cavity due to the lowest reflection loss on the BP face by precisely adjusting the horizontal and pitch angles of the output mirror M. And the other two wavelengths at 1112 nm and 1116 nm are suppressed due to the roundtrip reflection loss caused by non-zero reflectivity ($\sim 0.48\%$ at 1112 nm and $\sim 0.88\%$ at 1116 nm in the cavity, respectively).

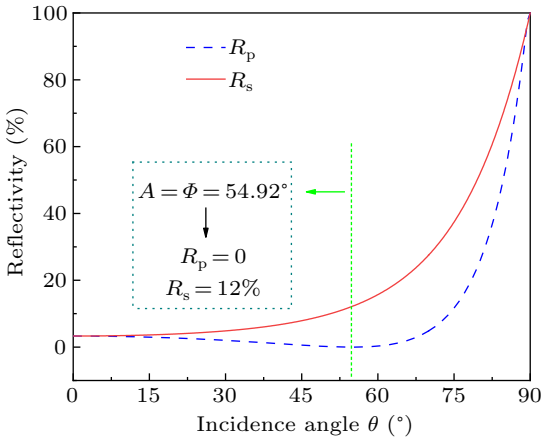


Fig. 3. Reflectance on the surface of BP with different θ values.

Meanwhile, BC is introduced where its transmission surface is perpendicular to the p-polarized 1123 nm laser. Leveraging the inherent birefringent effect, BC splits the p-polarized 1123 nm laser into an ordinary light (o-light) and an extraordinary light (e-light). After a single round-trip through BC, a phase delay $\Delta\varphi$ is induced between the o-light and e-light[27]

$$\Delta\varphi = \frac{2\pi}{\lambda}\cdot(n_{\rm o}-n_{\rm e})\cdot 2d = \frac{4\pi D(n_{\rm o}-n_{\rm e})}{\lambda}, \tag{6}$$

where $D = 2.5$ mm represents the thickness of BC. $\lambda = 1123$ nm represents the laser wavelength. $n_{\rm o}$ and $n_{\rm e}$ denote the refractive indices of the o-light and the e-light, respectively.

Rotating BC around the optical axis of the cavity, the p-polarized light at 1123 nm undergoes a 180° rotation after a single round trip through BC when the angle β between the p-polarized light at 1123 nm and the optical axis of BC becomes 45°, corresponding to a 2π multiple of $\Delta\varphi$:[28]

$$\Delta\varphi = 2m\pi, \tag{7}$$

where $m = 0, \pm1, \pm2, \pm3, \ldots$

Since the p-polarized direction has not changed, only the longitudinal modes at 1123 nm with $m = 0, \pm1, \pm2, \pm3, \ldots$ can achieve low-loss oscillation in the cavity. At 1123 nm, the remaining longitudinal modes will be suppressed. It should be emphasized that the round-trip transmittance of p- and s-polarized laser beams in the cavity after passing BC is given by the following equations:[29]

$$T_{\rm p} = \frac{1}{4}\left\{(1+q^4)\cdot\cos\left(\frac{1}{\Delta\varphi}\right) + \sqrt{(1+q^4)^2\cdot\cos^2\left(\frac{1}{\Delta\varphi}\right)-4q^4}\right\}^2, \tag{8}$$

$$T_{\rm s} = \frac{1}{4}\left\{(1+q^4)\cdot\cos\left(\frac{1}{\Delta\varphi}\right) - \sqrt{(1+q^4)^2\cdot\cos^2\left(\frac{1}{\Delta\varphi}\right)-4q^4}\right\}^2, \tag{9}$$

$$q = \frac{2n_i^*}{(n_i^*)^2+1}, \tag{10}$$

where $T_{\rm p}$ and $T_{\rm s}$ denote the transmittance of p- and s-polarized lights, respectively. n_i^* denote the refractive indices of BP made of optical quartz glass at wavelengths of 1112 nm, 1116 nm, and 1123 nm, respectively.

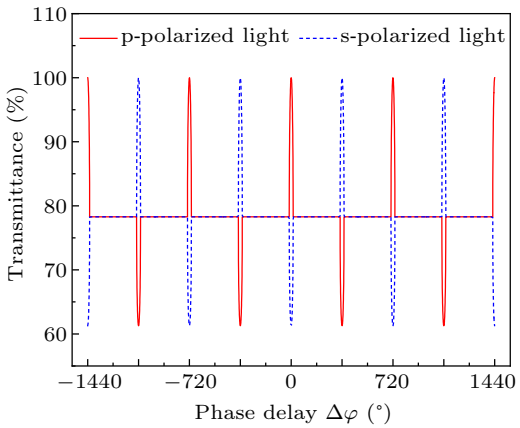


Fig. 4. Transmittance for the eigenvalues of the cavity included the BP and BC, plotted as a function of $\Delta\varphi$, for the case of $\beta = 45°$.

Figure 4 shows the solution of T_p and T_s a function of $\Delta\varphi$. The upper line corresponds to T_p and the lower one to T_s. These two lines join to form a single line at the angle of about 14° and the transmittance of about 78.3%. This figure indicates the zero round-trip loss at $\Delta\varphi = 2m\pi$ (m is even) for the 1123 nm p-polarized laser beam. However, the phase delays $\Delta\varphi^*$ of the two adjacent p-polarized spectral lines at 1112 nm and 1116 nm will not satisfy Eq. (7). The refractive indices of o- and e-light of quartz crystals at 1112 nm, 1116 nm and 1123 nm are ($n^*_{\text{o-1112}} = 1.5309$, $n^*_{\text{e-1112}} = 1.5446$), ($n^*_{\text{o-1116}} = 1.5308$, $n^*_{\text{e-1116}} = 1.5445$) and ($n^*_{\text{o-1123}} = 1.5307$, $n^*_{\text{e-1123}} = 1.5443$), respectively. According to Eqs. (6) and (7), it can be derived that the additional phase delays $\Delta\varphi^*$ of the 1112 nm and 1116 nm spectral lines with respect to 1123 nm after round-trip passage through BC are 6.5854° and 5.1988°, which correspond to a transmittance of $\sim 97.17\%$ and $\sim 98.28\%$, respectively. BC attaches a round-trip reflection loss of $\sim 2.83\%$ and $\sim 1.72\%$ for the two spectral lines 1112 nm and 1116 nm (m is zero or even), respectively. When m is odd, the three spectral lines at 1112 nm, 1116 nm, and 1123 nm are suppressed due to the high reflectivity (about 40%) when passing through BC. The above results indicate that both BP and BC have the capability to suppress oscillation of the 1112 nm and 1116 nm spectral lines in the cavity. The synergistic utilization of BP induces BC to exhibit greater reflective losses for the 1112 nm and 1116 nm spectral lines, thereby further enhancing the cavity's suppression capability towards these two lines. In summary, the combined use of BP and BC not only ensures that only the 1123 nm laser oscillates and is amplified in the cavity, but also reduces the number of longitudinal modes in the 1123 nm laser, thereby achieving filtering and noise reduction in the 1123 nm laser.

4.1. BP and BC are not placed in the cavity

When BP and BC are not used, a passively Q-switched pulsed laser based on cavity finely tuning is observed when the LD pump power reaches 1.26 W, as shown in Figs. 5(a)–5(d). Continuing to increase the LD pump power, the repetition frequency of the laser pulse train gradually increased while the pulse width was gradually compressed. This is attributed to the increasing trend of laser power density in the cavity with the increasing LD pump power, allowing the $Ti_3C_2T_x$-PVA film to reach the absorption saturation state for a shorter time period. When the LD pump power was increased to the maximum value of 5.1 W, the maximum average power of the passively Q-switched pulsed laser with a maximum repetition frequency of 909 kHz reached 365.2 mW, corresponding to an oblique efficiency of 9.5% and an optical to optical conversion efficiency of 7.1%, respectively. The narrowest pulse was 70 ns. However, the three spectral lights at 1112 nm, 1116 nm, and 1123 nm oscillated simultaneously in the cavity lacking frequency selection and filtering of BP + BC.

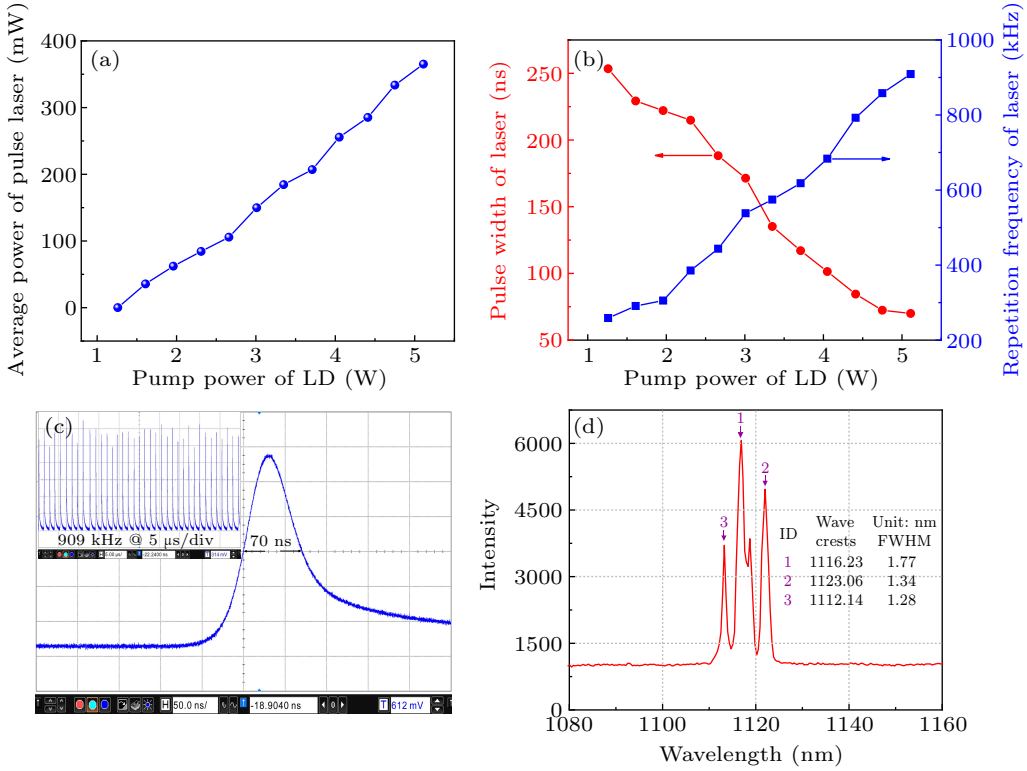


Fig. 5. Output characteristics of the passively Q-switched pulsed laser without frequency selection and filtering of BP + BC. (a) Average output power. (b) Repetition frequency and pulse width. (c) Pulse width of 70 ns at the maximum average output power of 365.2 mW. Inset: Pulse train with the repetition frequency of 909 kHz. (d) Measured spectrum.

Using a splitter mirror (with a transmittance of $\sim 96\%$ and a reflectivity of $\sim 4\%$ at 1123 nm), a power meter, an oscilloscope, and a PIN-type silicon photodiode, the power stability and laser noise of the passively Q-switched pulsed laser at 1123 nm were simultaneously measured at maximum output power. The duration and interval of the measurement were 4 h and 2 s, respectively. The power meter was used to measure the power instability of the transmitted pulsed laser at 1123 nm (Fig. 6(a)). In contrast, two PIN-type silicon photodiodes and an oscilloscope were employed to measure the laser noise of the reflected pulsed laser at 1123 nm (Fig. 6(b)). The silicon photodiode generated an electrical signal that was split in two. With an optical shutter blocking the laser beam, the electrical signal into the channel $1^{\#}$ (AC-coupled mode) of the oscilloscope represented background noise (area $\Gamma_{\text{B-RMS}}$ in Fig. 6(b), blue curve). Removing the optical shutter, the electrical signal into channel $1^{\#}$ represented total noise (area $\Gamma_{\text{T-RMS}}$ in Fig. 6(b), blue curve), including the laser noise of the pulsed laser at 1123 nm and background noise, while the electrical signal into channel $2^{\#}$ (DC-coupled mode) of the oscilloscope represented the absolute intensity of the pulsed laser at 1123 nm (area $\Gamma_{\text{I-RMS}}$ in Fig. 6(b), red curve). The power instability ρ and the noise $\Gamma_{\text{L-RMS}}$ of the passively Q-switched pulsed laser at the maximum average power were measured to be $\pm 5.23\%$ and 5.21% within a 4 h period using the following equations:[30,31]

$$\rho = \pm \frac{|P_{\text{MAX}} - P_{\text{MIN}}|}{2P_{\text{AM}}}, \tag{11}$$

$$\Gamma_{\text{L-RMS}} = \frac{\Gamma_{\text{T-RMS}} - \Gamma_{\text{B-RMS}}}{\Gamma_{\text{I-RMS}}}, \tag{12}$$

where P_{MAX}, P_{MIN}, and P_{AM} denote the maximum, minimum, and arithmetic mean values of the detected laser average power, respectively. $\Gamma_{\text{B-RMS}}$, $\Gamma_{\text{T-RMS}}$, and $\Gamma_{\text{I-RMS}}$ denote the RMS-background noise, the RMS-total noise, and the RMS-absolute intensity, respectively. The poor output stability indicates that it is necessary to suppress the oscillation of the 1112 nm and 1116 nm spectral lights in the cavity to achieve stable output of the passively Q-switched 1123 nm pulsed laser.

4.2. BP frequency selection in the cavity

A BP was inserted into the above unfiltered cavity, and its horizontal angle was precisely adjusted to match the Brewster angle (54.92° at 1123 nm). As shown in Figs. 7(a)–7(d), the presence of the spectrum line at 1123 nm only in the collected laser spectrum indicates that the BP suppresses intracavity oscillations at 1112 nm and 1116 nm. The insertion of BP increased the threshold of LD pump power from 1.26 W to 1.86 W. However, the effective suppression of the intracavity oscillations for the spectral lines at 1112 nm and 1116 nm mitigates mode competition and enhances the gain of the spectral line at 1123 nm. At 1123 nm at the maximum LD pump power of 5.1 W, the passively Q-switched pulsed laser had the maximum average output power of 405.3 mW, the maximum repetition frequency of 1.01 MHz, the narrowest pulse width of 63 ns, and the narrowest line width of 0.95 nm. The measured ρ and $\Gamma_{\text{L-RMS}}$ decreased to $\pm 1.84\%$ and 2.55% after continuous monitoring for 4 h with an interval of 2 s, respectively.

4.3. Frequency selection and filtering of BP + BC in the cavity

On the basis of BP frequency selection, a BC was inserted into the cavity. The horizontal and pitch angles of BC were precisely adjusted with the aim of ensuring $\beta = 45°$. BC filtering reduces the number of longitudinal modes in the cavity, thereby alleviating mode competition between longitudinal modes in the passively Q-switched pulsed laser at 1123 nm. On the one hand, the longitudinal modes that satisfy Eq. (7) and m is zero or even can achieve higher gain, while on other hand the combination of BP and BC is more effective in suppressing intracavity oscillation of spectral lines at 1112 nm and 1116 nm. As shown in Figs. 9(a)–9(d), although BC further increased the pump threshold of LD to 2.84 W, the passively Q-switched pulsed laser at 1123 nm obtained the better output characteristics. As a result, the average power of the passively Q-switched pulsed laser at 1123 nm with a maximum repetition frequency of 1.09 MHz reached 457.9 mW under the maximum LD pump power of 5.1 W. Meanwhile, a narrowest pulse width of 56 ns and a narrowest spectral line width of 0.65 nm were measured. This is because, the power density of the passively Q-switched pulsed laser at 1123 nm with partial longitudinal mode suppressed significantly increases, which allows the $Ti_3C_2T_x$-PVA film to reach absorption saturation at a shorter period and higher frequency.[32,33] At higher power density, the time required for the excited energy level of the $Ti_3C_2T_x$-PVA film to enter saturation is shorter, thus obtaining higher repetition frequency and shorter pulse width.[34] Continuously monitoring the maximum average power of the passively Q-switched pulsed laser at 1123 nm for 4 h with an interval of 2 s, the ρ and $\Gamma_{\text{L-RMS}}$ were reduced to $\pm 0.92\%$ and 0.89%, respectively. The results demonstrate that the frequency selection and filtering of BP + BC have jointly suppressed the noise in the passively Q-switched pulsed laser at 1123 nm by reducing both the number of wavelengths and longitudinal modes in the cavity. Considering the adopted thermal management measures, the stable output of the passively Q-switched laser over duration of 12 h also demonstrates the excellent operational reliability of the $Ti_3C_2T_x$-PVA film as SA from another perspective.

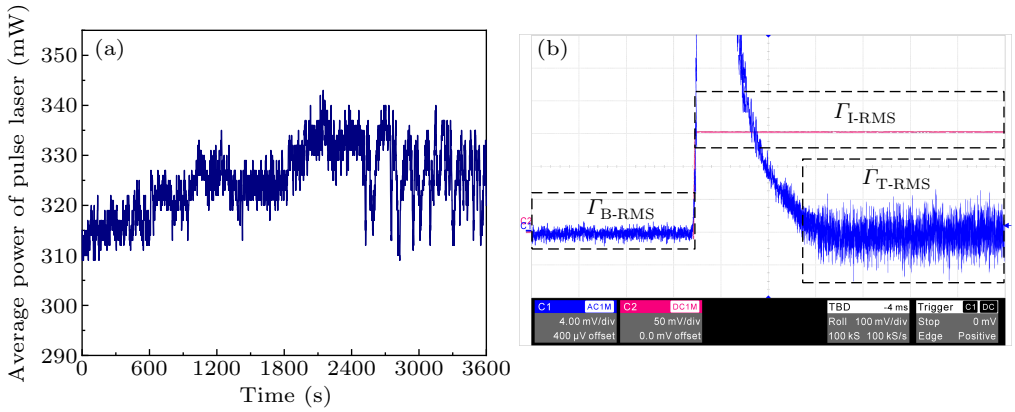


Fig. 6. Stability of pulsed laser at maximum average output power in a 4 h period without frequency selection and filtering of BP+BC. (a) Power instability. (b) RMS-laser noise.

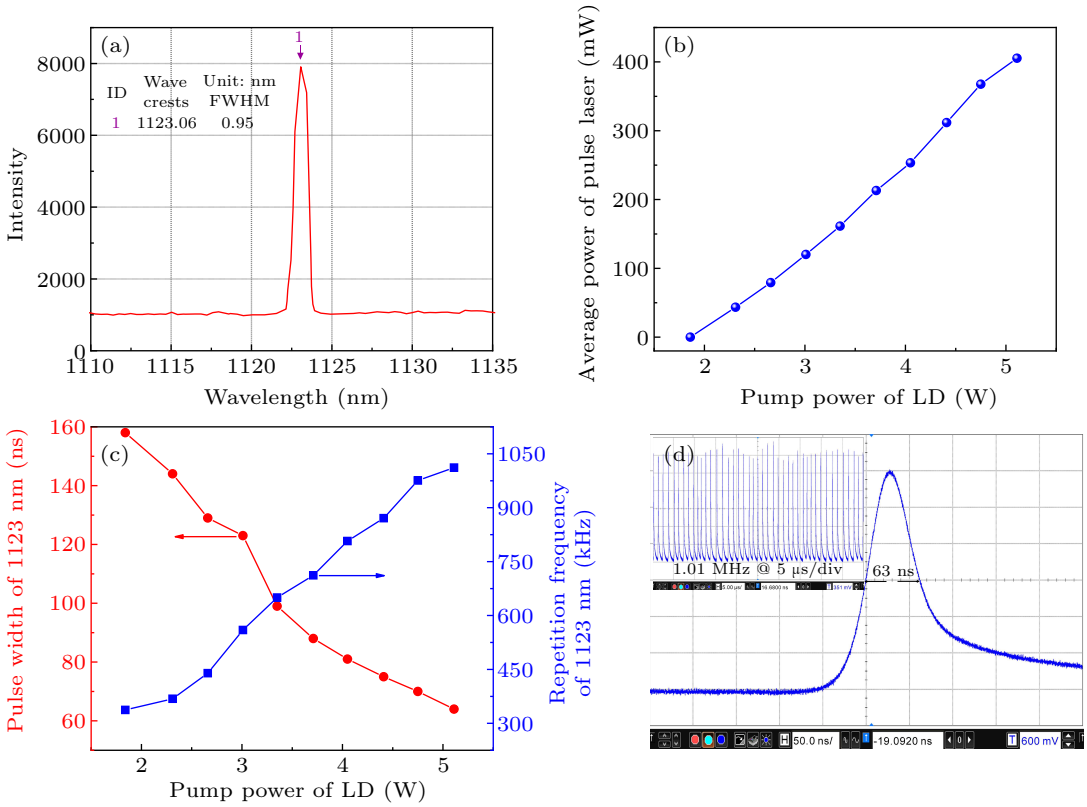


Fig. 7. Output characteristics of the passively *Q*-switched pulsed laser at 1123 nm using BP frequency selection. (a) Measured spectrum. (b) Average output power. (c) Repetition frequency and pulse width. (d) Pulse width of 63 ns at the maximum average output power of 405.3 mW. Inset: Pulse train with the repetition frequency of 1.01 MHz.

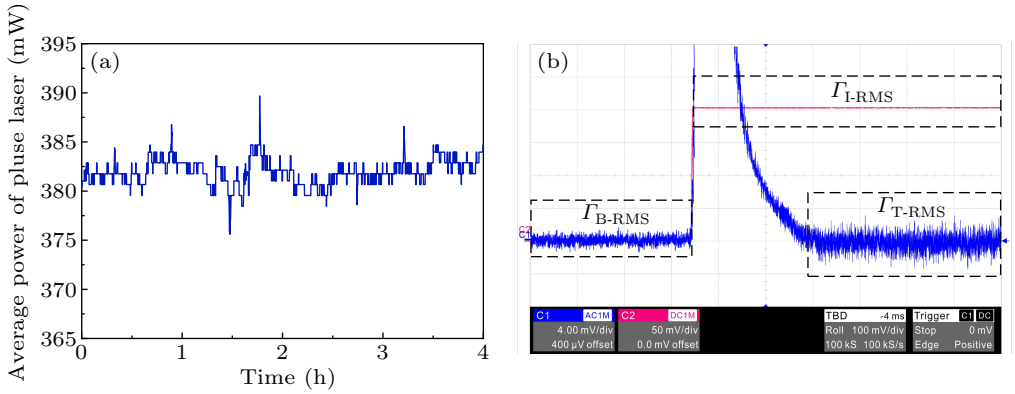


Fig. 8. Stability of pulsed laser at maximum average output power in a 4 h period using BP frequency selection. (a) Power instability. (b) RMS-laser noise.

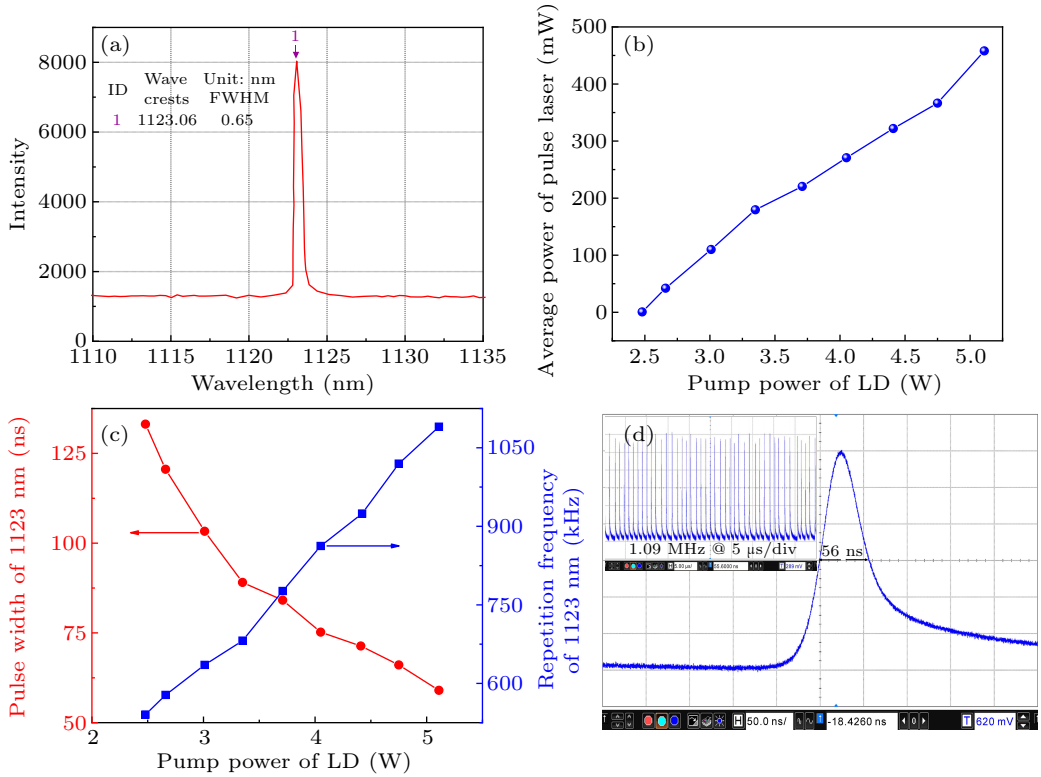


Fig. 9. Output characteristics of the passively Q-switched pulsed laser at 1123 nm using frequency selection and filtering of BP + BC. (a) Measured spectrum. (b) Average output power. (c) Repetition frequency and pulse width. (d) Pulse width of 56 ns at the maximum average output power of 457.9 mW. Inset: Pulse train with the repetition frequency of 1.09 MHz.

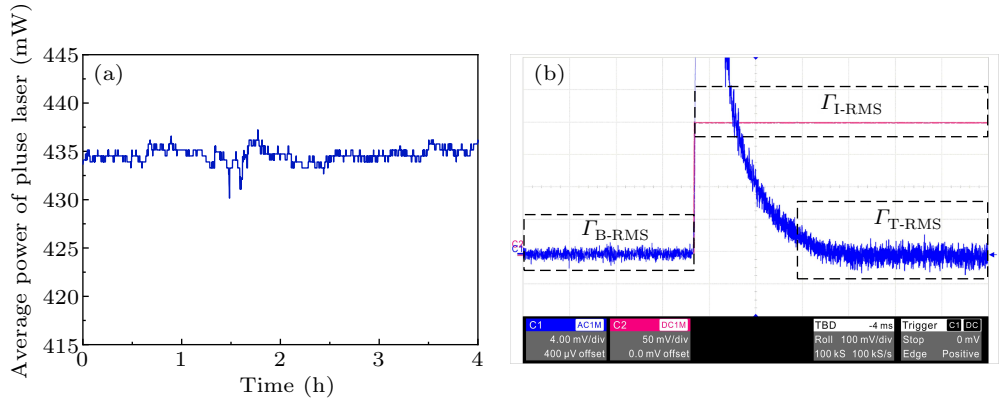


Fig. 10. Stability of pulsed laser at maximum average output power in a 4 h period with frequency selection and filtering of BP + BC. (a) Power instability. (b) RMS-laser noise.

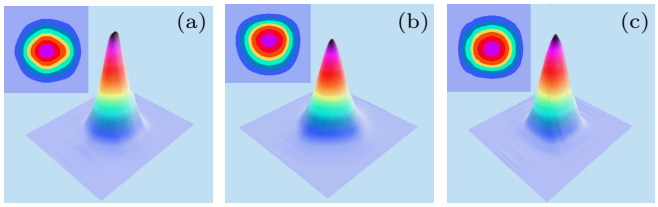


Fig. 11. 2D and 3D near-field beam profiles of the passively Q-switched 1123 nm pulsed laser. (a) Without frequency selection and filtering of BP + BC. (b) With frequency selection of BP. (c) With frequency selection and filtering of BP + BC. Insets: 2D near-field beam profiles.

In addition, the beam quality M^2 factors of the three passively Q-switched 1123 nm pulsed laser beams, as measured by a laser beam quality analyzer were found to be ($M_x^2 = 5.814$, $M_y^2 = 5.428$), ($M_x^2 = 3.466$, $M_y^2 = 3.288$), and ($M_x^2 = 2.505$, $M_y^2 = 2.177$), respectively. The 2D and 3D images of the near-field beam are shown in Fig. 11. The smaller beam quality M^2 factors further confirm that the "frequency selection and filtering of BP + BC" contributes to the improvement of beam quality for the passively Q-switched 1123 nm pulsed laser.

5. Conclusion

In this work, a solid-state pulsed laser at 1123 nm with high repetition frequency, high power stability and low laser noise based on a $Ti_3C_2T_x$-PVA film passively Q-switching combined with "frequency selection and filtering of BP + BC was proposed. The maximum average power of 457.9 mW,

maximum repetition rate of 1.09 MHz, narrowest pulse width of 56 ns, and narrowest line width of 0.65 nm were obtained simultaneously, with corresponding the power instability and the laser noise only at ±0.92% and 0.89%, respectively. Our first proposed "$Ti_3C_2T_x$-PVA film passively *Q*-switching" combined with "frequency selection and filtering of BP + BC" technology path will be of great significance in promoting the wider application of passively *Q*-switched pulsed laser at 1123 nm with high repetition frequency, high power stability, and low noise in the fields of biotechnology, laser display, frequency conversion, and high-resolution optical sensing.

Acknowledgments

Project supported by the Serving Local Special Project of Shaanxi Provincial Department of Education of China (Grant No. 19JC040) and the National Natural Science Foundation of China (Grant No. 61905193).

References

[1] Räikkönen E, Kimmelma O, Kaivola M and Buchter S C 2008 *Opt. Commun.* **281** 4088
[2] Singh S, Smith R G and Van Uitert L G 1974 *Phys. Rev. B* **10** 2566
[3] Czeranowsky C, Heumann E and Huber G 2003 *Opt. Lett.* **28** 432
[4] Liu W B, Zhang D, Zeng Y P, Li J, Pan Y B, Guo J K, Bo Y, Peng Q J and Xu Z Y 2012 *Ceram. Int.* **38** 6969
[5] Li C Y, Peng Q J, Wang B S, Bo Y, Cui D F, Xu Z Y, Feng X Q and Pan B 2011 *Appl. Phys. B* **103** 285
[6] Chen Y F and Lan Y P 2004 *Appl. Phys. B* **79** 29
[7] Cai Y P, Ding J, Bai Z X, Qi Y Y, Wang Y L and Lu Z W 2022 *Opt. Laser Technol.* **152** 108113
[8] Gao J, Dai X J, Zhang L, Sun H X and Wu X D 2013 *J. Opt. Soc. Am. B* **30** 95
[9] Shen H B, Wang Q P, Zhang Y X, Liu Z J, Bai F, Gao L, Lan W X, Wu Z G, Wang W T and Zhang Y G 2013 *Laser Phys.* **23** 035402
[10] Li Ping, Chen X H, Zhang H N, Ma B M and Wang Q P 2011 *Appl. Phys. Express* **4** 092702
[11] Liu Y, Ni J S, Shang Y, Qi H F and Zhao W N 2018 *J. Russ. Laser Res.* **39** 608
[12] Li C Y, Bo Y, Xu J L, Tian C Y, Peng Q J, Cui D F and Xu Z Y 2011 *Opt. Commun.* **284** 4574
[13] Liu H and Ma L G 2012 *Chin. Phys. B* **21** 104208
[14] Wang Z F, Wang X Z, Cai M C, Bu Y K, Chen L J and Cai G X 2014 *Opt. Commun.* **330** 143
[15] Chang A, Wu C T, Yao W M, Wang P, Chen J S, Tan H M, Tian Y B, Wu X D and Gao J 2023 *Microw. Opt. Technol. Lett.* **65** 1255
[16] Feng X Y, Ding B Y, Liang W Y, Zhang F, Ning T Y, Liu J and Zhang H 2018 *Laser Phys. Lett.* **15** 085805
[17] Hao Q Q, Liu J J, Zhang Z, Zhang B, Zhang F, Yang J M, Liu J, Su L B and Zhang H 2019 *Appl. Phys. Express* **12** 085506
[18] Tian Q Y, Yin P, Zhang T, Zhou L B, Xu B, Luo Z Q, Liu H L, Ge Y Q, Zhang J, Liu P and Xu X D 2020 *Nanophotonics* **9** 2495
[19] Wang C, Peng Q Q, Fan X W, Liang W Y, Zhang F, Liu J and Zhang H 2018 *Chin. Phys. B* **27** 094214
[20] Sarycheva A and Gogotsi Y 2020 *Chem. Mater.* **32** 3480
[21] Tai H L, Duan Z H, He Z Z, Li X, Xu J L, Liu B H and Jiang Y D 2019 *Sens. Actuators B Chem.* **298** 126874
[22] He Z W, Zheng Y, Liu H Y, Li M K, Lu H, Zhang H Z, Feng Q L and Mao D 2019 *Chin. Opt. Lett.* **17** 020004
[23] Wang X B, Xu X J, Li X and Lu Q S 2007 *Appl. Opt.* **46** 5237
[24] Sun Y X, Bai Y, Li D, Hou L, Bai B, Gong Y Z, Yu L L and Bai J T 2017 *Opt. Express* **25** 21037
[25] Bhattacharya K 2022 *Eur. J. Phys.* **43** 035305
[26] Peiponen K E and Vartiainen E M 2006 *J. Opt. Soc. Am. B* **23** 114
[27] Huang B, Wang Y and Mao C 2020 *IEEE Access* **8** 25764
[28] Bai Y, Chen Z H, Li B, Yang S Y, Liu H and Zhou J F 2022 *Laser Phys.* **32** 125803
[29] Nagai H, Kume M, Ohta I, Shimizu H and Kazumura M 1992 *IEEE J. Quantum Electron.* **28** 1164
[30] Bai Y, Bai B, Li D, Sun Y X, Li J l, Hou L, Hu M X and Bai J T 2018 *High Power Laser Sci. Eng.* **6** e4
[31] Bai B, Bai Y, Li D, Sun Y X, Li J L and Bai J T 2018 *Chin. Opt. Lett.* **16** 031402
[32] Liu Y, Zhang S S, Cong Z H, Men S J, Guan C, Xie Y Y and Liu Z J 2021 *Crystals* **11** 58
[33] Zhu P F, Zhang C M, Song P, Bai L and Yao Y 2015 *Opt. Spectrosc.* **118** 623
[34] Wang J, Xie L, Wang Y H, Lan Y, Wu P F, Lv J, Zhang G D, Miao Z C and Cheng G H 2023 *Infrared Phys. Technol.* **129** 104580